HAL
open science

Structural correlations and chemistry of the Na3AlF6 – SiO2 melt as an electrolyte for the solar grade silicon (SOG – Si) electrowinning

František Šimko, Aydar Rakhmatullin, Michal Korenko, Catherine Bessada

▶ **To cite this version:**

František Šimko, Aydar Rakhmatullin, Michal Korenko, Catherine Bessada. Structural correlations and chemistry of the Na3AlF6 – SiO2 melt as an electrolyte for the solar grade silicon (SOG – Si) electrowinning. Journal of Molecular Liquids, 2021, 328, pp.115453. 10.1016/j.molliq.2021.115453 . hal-03382753

HAL Id: hal-03382753

https://hal.science/hal-03382753v1

Submitted on 19 Oct 2021

HAL is a multi-disciplinary open access archive for the deposit and dissemination of scientific research documents, whether they are published or not. The documents may come from teaching and research institutions in France or abroad, or from public or private research centers.

L'archive ouverte pluridisciplinaire **HAL**, est destinée au dépôt et à la diffusion de documents scientifiques de niveau recherche, publiés ou non, émanant des établissements d'enseignement et de recherche français ou étrangers, des laboratoires publics ou privés.

Structural Correlations and Chemistry of the Na_3AlF_6–SiO_2 Melt as an Electrolyte for the Solar Grade Silicon (SOG−Si) Electrowinning

František Šimko[a,b,*], Aydar Rakhmatullin[c], Michal Korenko[a,b], and Catherine Bessada[c]

[a] *Institute of Inorganic Chemistry, Slovak Academy of Sciences, Dúbravská cesta 9, 845 36 Bratislava, Slovakia*
[b] *Centre of Excellence for advanced Materials Application - CEMEA, Slovak Academy of Sciences, Dúbravská cesta 5807/9, 845 11 Bratislava, Slovakia*
[c] *Conditions Extremes et Materiaux: Haute Temperature et Irradiation (CEMHTI-CNRS), 1D avenue de la Recherche Scientifique CS 90055, 45071 Orleans cedex 2, France*

**Corresponding author: František Šimko, Institute of Inorganic Chemistry, Slovak Academy of Sciences, Dúbravská cesta 9, 845 36 Bratislava, Slovakia, e-mail: uachsim@savba.sk, tel.: 00421-2-59410495*

ABSTRACT

Molten system Na_3AlF_6−SiO_2 was examined by high temperature NMR. Further characterizations of the samples prepared by Rapid Solidification Processing (RSP) technique and by spontaneous solidification were performed by X–ray diffraction and solid state NMR. The high solubility of SiO_2 in molten cryolite and the immiscibility phenomenon were observed. Using thermogravimetric analysis, weight losses were detected, which could be attributed to the formation of the volatile products. The results of the present study are the evidence that SiO_2 reacts with molten Na_3AlF_6 under the formation of the volatile SiF_4, non−volatile NaF, and alumino−silicate $AlSi_3O_8^-$ species. NMR spectroscopy coupled with diffraction−based methods was proved as a promising approach to obtain information about the structure and chemistry of this rather complex system.

Keywords: solid grade silicon, high temperature NMR, Na_3AlF_6, SiO_2, alumino–silicates

1. Introduction

Solar power energy is the most prevalent form of a renewable energy. It is not yet apparent what portion of our energy needs will be ultimately based on the sunshine, although it has a potential to definitely far transcend the total energy demand of humankind on the globe.

Over 90 % of today`s photovoltaic cells still use silicon as conversion material. The reason is its abundance (Si constitutes 27 mass % of earth's crust), non−toxicity, acceptable band gap and reasonable energy conversion efficiency (around 20 %) [1-3]. One of the current hurdles against solar energy becoming a major contributor to the energy basket is still its high cost. An increasing attention has been thus paid to the production of solar grade silicon (SOG−Si) at low cost.

The understanding of the relations between the structure and chemistry inside the molten electrolyte systems (nature of ionic electroactive species, product of thermal dissociation, co–ordination chemistry, *etc.*) and their physico−chemical properties (conductivity, viscosity, density, phase equilibria, *etc.*) is essential for the industrial application, yet necessary information in this area is still very limited. Some studies on electrochemistry of some fluoride and chloride systems have been published in the seventies and eighties of the 20th century [4−6]. Also, in recent years, one can see an increasing interest in this field [7–21].

Previous screening in between the several molten salt electrolytes has pointed out that, with respect to the deposited material purity and process current efficiency, the cryolite–based melts are promising media for the electrowinning of silicon [22–23]. The process has not yet been, however, successfully commercialized due to the rather high melting point of silicon (1412 °C), prohibiting the production of liquid primary silicon at the temperatures usual for cryolitic electrolytes (*ca* 1000 °C). In addition, an accurate comprehension of the physico–chemical behavior and the structure of different cryolite–based electrolytes (including the knowledge of the electroactive species), what is vital for industrial application, is also very scarce [24–28].

Although physico-chemical behavior of the various molten cryolite systems is the subject of a longtime inquiry due to the Hall–Heroult technology, data regarding the physico-chemical properties of the particular system Na_3AlF_6−SiO_2 are not only rather limited, but also available only for a small concentration range of silica.

Batashev and Zhurin [29] were the very first who investigated the molten system Na_3AlF_6–SiO_2. These authors have found by visual observations the eutectic point in the system Na_3AlF_6–SiO_2 at approximately 3 wt. % SiO_2 (9.75 mole %) and 980 °C. Likewise, a narrow field of solid solution of SiO_2 in cryolite was postulated on the cryolite side of the binary phase diagram. On the SiO_2 side (beyond the eutectic point), an area of immiscibility of the two liquid phases was found. However, these results, according Grjotheim and Matiašovský [25], have to be considered just as preliminary, and still need to be verified.

The data related to the system Na_3AlF_6−SiO_2 was later reviewed by Grjotheim *et al.* [30]. The authors concluded that silica reacts with cryolite (Na_3AlF_6) or AlF_3 with the formation of volatile SiF_4:

$$4Na_3AlF_6 + 3SiO_2 \rightarrow 3SiF_4 + 12NaF + 2Al_2O_3 \quad (1)$$

or

$$Na_3AlF_6 + SiO_2 \rightarrow SiF_4 + 12NaAlO_2 + 2NaF \quad (2)$$

and

$$4AlF_3 + 3SiO_2 \rightarrow 3SiF_4 + 2Al_2O_3 \quad (3)$$

The rates of these reactions are based on the authors, however, rather slow, and thus the changes in chemical composition of the melts are almost negligible.

The phase equilibria in the isothermal section of the system Na_3AlF_6−Al_2O_3−SiO_2 at 1010 °C were investigated by Weill and Fyfe [28]. The authors have found that the solubility of SiO_2, which is in pure Na_3AlF_6 (1010 °C) less than 5 wt. % (15.53 mole %), increases with increased concentration of Al_2O_3 in the melt. The paper has also reported that the changes in the composition of the melt, due to the formation of volatile SiF_4, were negligible and did not significantly affect the final composition of the melt after precipitation. It should be pointed out that the experiments [28] were carried out in a closed system (Pt vial) where the reaction equilibrium likely shifted to the left. In the open systems SiF_4 can, on the other hand, escape away of the reaction vessel, and the losses of fluorides caused by the reactions (1 or 2) can be detected and can cause more significant change of the reactant`s composition.

Fellner and Matiašovský [31] were determining the influence of the different melt compositions on the losses of SiO_2 (and subsequently on the losses of fluorine) in the Na_3AlF_6−SiO_2 melt. The change of Gibbs energy in the reaction (1) is positive (ΔG_R^0 (1300 K) = 506.81 kJ/mol) so one can expect that the equilibrium of the reaction would be shifted to the left−hand side. The authors mentioned rather high losses of fluorides (in the open reaction systems) likely caused by the reaction (1 or 2 and 3). It was found that the components in the system react with the formation of volatile SiF_4. The formation of SiF_4 was subsequently determined analytically [31].

The main aim of this work is focused on the behavior of SiO_2 in molten Na_3AlF_6. Our goal is to find out the structure and the form of all entities; ionic, non−ionic, complex, or polymerized in molten cryolite−silica melts. High Temperature (HT) Nuclear Magnetic Resonance (NMR) provides direct information about the number and the nature of present ions in the melt as well as local symmetry of the present constituents [32−35]. Rapid Solidification Processing (RSP) allows us to prepare the solidified melt samples with an internal structure as close as possible to a liquid state. Such prepared samples can be then easily analyzed by a whole spectrum of conventional room temperature spectral techniques.

A frequent presence of different disordered solids is well known as a problem in resolving the structure of SiO_2 containing systems. To understand and to comprehend the structure of disordered solids is a difficult task taking into account a missing long–range periodicity and the impossibility to make use of standard diffraction techniques. One of the main experimental methods to determine short–range structures in glasses and amorphous materials is high resolution solid–state NMR spectroscopy.

2. Experimental

2.1. Chemicals and preparation of samples

Chemicals: The chemicals sodium hexafluoroaluminate (Na_3AlF_6), and silicon dioxide (SiO_2) were analytical grade and purchased commercially. The CAS Registry Nos., suppliers, and mass fractions are listed in Table 1. The chemicals were stored in glove box Jacomex GP concept with autonomous purification system, at atmosphere of inert argon gas. All the chemicals were used directly for samples preparation. The weighing, homogenization in mortar and preparation of each individual sample were performed in a glovebox.

Table 1. CAS Registry Number, Mass Fraction and Purity of used Chemicals and materials.

component	CAS Reg. No.	suppliers	purity
Sodium hexafluoroaluminate Na_3AlF_6	13775-53-6	Alfa Aesar by Thermo Fischer Scientific GmbH, Germany	99.90%, powder
Silicon dioxide, SiO_2	7631-86-9	JMC (Johnson Matthey Chemicals Limited)	99.90%, powder
BN crucible with lid, BN, for high-temperature NMR measurements	10043-11-5	P Vision-ABC France	99.99%, Crucible Ø 9, hole Ø 2.5×7 mm deep
BN crucible for weight-loss measurements	10043-11-5	Saint-Gobain Construction Products, s.r.o., USA	99.99%, Crucible Ø 30, hole Ø 25×70 mm deep
Argon, Ar	7440-37-1	SIAD, Slovakia	99.999%, gas
Platinum/10rhodium, PtRh10	11107-71-4	Safina, Slovakia	90%Pt10%Rh, crucible
Sintered aluminium oxide, Al_2O_3	1344-28-1	Morgan Advanced Materials Haldenwanger GmbH, Germany	99.7%, sintered tubes
Sodium chloride ultrapure, NaCl	7647-14-5	Alfa Aesar by Thermo Fischer Scientific GmbH, Germany	99.9%, powder
Sodium fluoride, NaF	7681-49-4	Alfa Aesar by Thermo Fischer Scientific GmbH, Germany	99.9%, powder

For individual purpose (spontaneously cooled samples, rapid solidified samples, high-temperature NMR measurements), the mechanically homogenized powder mixtures of Na_3AlF_6 and SiO_2 (in a mole content 0, 5, 25 and 50 mole % of SiO_2) were prepared in a glovebox, in an argon inert environment.

Preparation of spontaneously cooled samples**:** Individual samples were synthetized by direct reaction in molten state. 10.0000 grams of each mixture were individually placed in a Pt crucible and heated in a resistance furnace from room temperature up to 1025°C at a heating rate of 5 K/min under 0.2 MPa of argon atmosphere. The holding time was 100 min. The temperature control and the data processing were performed using a computerized measuring device (multicomponent model for thermal analysis data collections National Instruments, where the data collections run online under Labview software). The temperature of the samples was controlled by a Pt-PtRh10 thermocouple, calibrated on the melting points of highly pure NaCl and NaF. The accuracy of the temperature difference measurement between the temperatures of primary crystallizations of the given mixtures was (±1 ^{o}C). After melting, the samples were then spontaneously cooled down to room temperature at a rate of 7 ^{o}C/min. The samples were then homogenized in glovebox and ready for analysis.

Preparation of rapid solidified (RSP) samples: For RSP experiments the samples with the same composition and were pressed into the form of tablets (30 grams). The RSP apparatus

(more specifically for the melt spinning method) consisted of an induction heating coil and a rotating cooling Cu-wheel. The samples, in the form of pressed pellets, were placed in a graphite crucible glued into a quartz tube. At the bottom of the crucible there was a small orifice for the outflow of melt. The distance between the orifice and the rotating cylinder was approximately 0.2 mm. The quartz housing tube with the crucible and sample was filled with Ar, to ensure an inert atmosphere. The apparatus arrangement permitted the solidification of the individual melts, heated on 1025°C, from the molten (above the melting point) to the solid state at a cooling rate of about 10^6 K s^{-1}. General details of the techniques may be found elsewhere [36, 37].

2.2. High–temperature and Solid–state NMR analysis

The different mixtures of Na_3AlF_6 and SiO_2 (α–quartz) were prepared in a glove box under dried argon atmosphere and mixed well. For HT NMR measurements, approximately 60 mg of the different mixtures were put into tightly closed high purity boron nitride (BN) crucibles to avoid any contamination [33].

All NMR measurements have been carried out using Bruker Avance 400 (9.4 T) NMR spectrometer. The HT NMR spectra have been acquired using the laser–heated NMR system, developed in CEMHTI Orleans [33]. The BN crucible containing the 100 mg of measuring sample is placed inside the radiofrequency coil into the NMR probe. To ensure a good homogeneous heating, the top and the bottom of the crucible are heated by a CO_2 laser (Coherent Diamond 250 W) passing axially through the NMR probe. The temperature is being controlled by laser power and during the experiment was kept on 1025 ^{o}C, for all measured salt mixture. The laser system was previously calibrated by a direct measurement of the temperature inside the NMR probe by a thermocouple. The melting point of the sample is clearly detected by the modification of the shape and width of the NMR line (Fig. 1), using single pulse excitation consisting of 20 μs pulses, recycle delays of 500 ms and 16 – 256 scans to obtain a reliable signal–to–noise ratio.

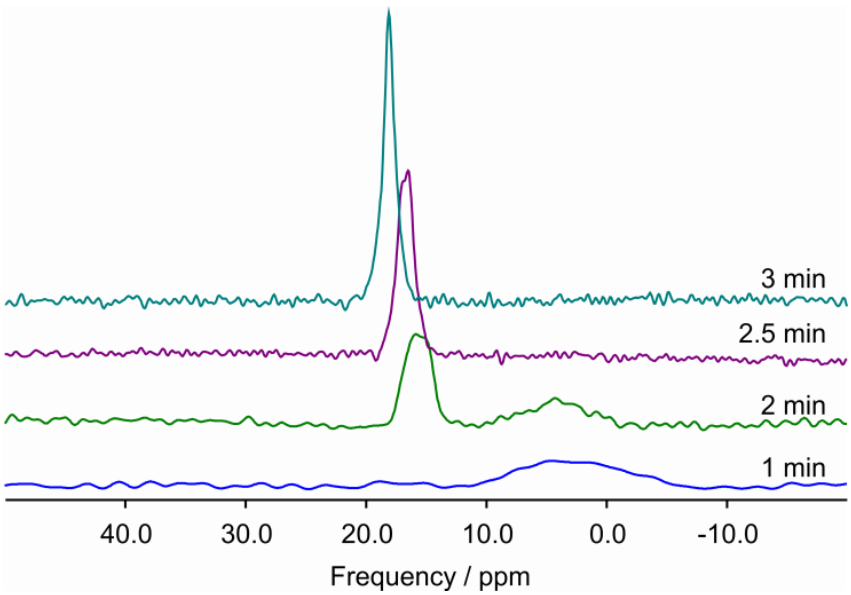

Fig. 1. ^{27}Al HT-NMR spectra of Na_3AlF_6 measured after 1, 2, 2.5, and 3 minutes from the start of heating.

At room temperature, magic angle spinning (MAS) NMR spectra were acquired using MAS probes from Bruker. ^{27}Al, ^{23}Na, and ^{19}F spectra were collected with 2.5 mm diameter rotors at the rotor frequencies of 30 kHz and ^{29}Si spectra with 7 mm diameter rotors at the rotor frequencies of 6 kHz. In order to ensure good excitation conditions for both quadrupolar nuclei ^{27}Al, and ^{23}Na, very short pulses of 0.5 μs were used with recycle times of 500 ms. For ^{19}F and ^{29}Si, $\pi/2$ pulse widths were 1.0 μs and 4.1 μs, respectively, and recycle delay was $5\times T_1$. Around 128 scans were acquired for ^{19}F experiments, and up to 1024 for ^{27}Al, ^{23}Na, and ^{29}Si. The reported chemical shifts are referenced to 1 M solutions of NaCl, $Al(NO_3)_3$ for ^{23}Na and ^{27}Al, respectively; TMS and $CFCl_3$ for ^{29}Si and ^{19}F, respectively. The NMR parameters (chemical shifts, line widths, quadrupolar coupling parameters) were fitted to the experimental spectra by means of a DMfit2013 program [38].

2.3. Weight–loss measurements

Weight–losses caused by the melting of the system were determined gravimetrically and by means of X–ray fluorescence analysis (XRF, ARL ADVANT´X 3600 W). The samples of the composition (Na_3AlF_6 – x mole % SiO_2, x = 0 – 40) and weight (30.0 ± 0.01) g were in the first step heated in boron nitride crucible up to 1020 °C in an argon inert atmosphere. The heating rate was 8 – 9 °C/min. After reaching the temperature, the samples were kept at this constant temperature for one hour and then spontaneously cooled at 7 °C/min to room temperature. The losses were *ex–post* recorded gravimetrically and the composition of the solidified samples was determined by XRF. The XRF device was firstly calibrated on the same system. The several solid samples have been prepared with the different composition of SiO_2 for the calibration beforehand. The uncertainty of the gravimetric weight-loss measurement was estimated as 0.1 %. The uncertainty of the XRF weight-loss measurement was estimated (based on the calibration) as 3 %.

2.4. X–ray measurements

All solidified samples were grounded to fine powders, and they were then mounted on foils (PANalytical B.V., X-ray film Polyimide 9430 500 21011). To collect the X–ray patterns, a transmission Stoe Stadi P diffractometer equipped with a linear PSD and a curved Ge(111) primary beam monochromator, was used. X–ray diffraction patterns were recorded within the interval of 10 °–80 ° in steps of 0.02° 2θ using Co Kα1 radiation. Phase analysis was performed using X'Pert HighScore Plus PANalytical software with the PDF2 2011 database.

2.5. Rapid solidified processing (RSP)

The rapidly solidified samples were prepared with a different amount of SiO_2 (5, 25 and 50 mole % of α–quartz). The RSP apparatus consisted from the inductive furnace and the rotating metal cylinder. Inside the inductive furnace was a quartz tube within the graphite

crucible with the samples (30 g). At the bottom of the graphite crucible was a small hole for the outflow of the melt. The distance between the hole and the rotating cylinder was *ca* 1 millimeter. A nitrogen inert atmosphere was used inside the furnace. The apparatus arrangement permitted the solidification process (from 100 °C above the melting point to the solid state) by a cooling rate at the interval of $10^5 - 10^6$ °C/s. Further general details of the technique may be found elsewhere [36, 37].

3. Results and Discussion

3.1. High temperature NMR analysis

The NMR spectra acquired in the molten state consist in a single Lorentzian line, characteristic of a rapid exchange at the timescale of NMR between the different atomic configurations around the observed nucleus. The measured chemical shift is thus the average of the individual chemical shifts of the different species.

Figure 2 shows an evolution of the shape of ^{27}Al spectra with the composition of silica. The evolution of the chemical shifts with silica content is reported for all nuclei ^{19}F, ^{23}Na, and ^{27}Al in Figure 3 and Table 2. The isotropic chemical shift of all three isotopes has a similar evolution with the increasing concentration of SiO_2 in melt. The whole spectra can be divided into two different parts. In the first part, one can see a continuous linear increasing of all three chemical shifts over the composition range from 0 to 32.5 mole % of SiO_2. The typical line widths (full width at half maximum, FWHM) are similar of an order between 90 and 160 Hz.

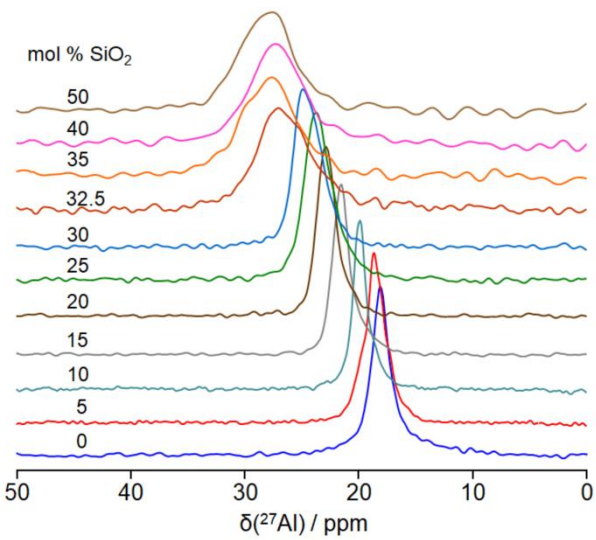

Fig. 2. ^{27}Al HT–NMR spectra as a function of SiO_2 concentration, measured at 1025 °C.

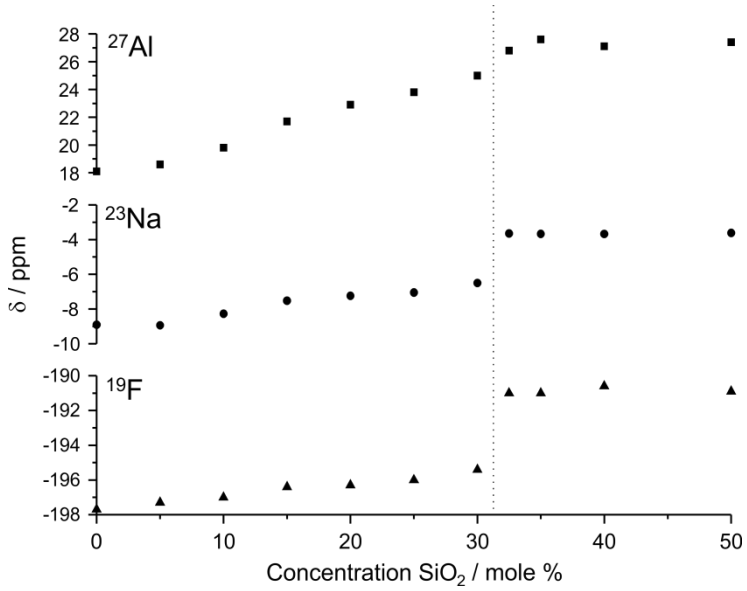

Fig. 3. ^{27}Al, ^{23}Na and ^{19}F chemical shifts evolution for Na_3AlF_6–SiO_2 melts, at 1025 °C.

Table 2. ^{7}Al, ^{23}Na and ^{19}F experimental chemical shifts and FWHM for Na_3AlF_6–SiO_2 melts, at 1025 °C.

Mole %	^{27}Al		^{23}Na		^{19}F	
SiO_2	δ_{iso} / ppm	FWHM / Hz	δ_{iso} / ppm	FWHM / Hz	δ_{iso} / ppm	FWHM / Hz
0	18.1	115	-8.9	82	-197.7	90
5	18.6	114	-8.9	80	-197.3	91
10	19.8	85	-8.3	86	-197.0	91
15	21.7	102	-7.5	82	-196.4	97
20	22.9	110	-7.2	97	-196.3	95
25	23.8	159	-7.1	93	-196.0	107
30	25.0	156	-6.5	90	-195.4	103
32.5	26.8	323	-3.7	177	-191.0	217
35	27.6	322	-3.7	163	-191.0	230
40	27.1	314	-3.7	180	-190.6	342
50	27.4	338	-3.6	176	-190.9	238

Standard uncertainties u are u(δ) = ± 0.5 ppm, u(FWHM) = 10 Hz

It can be seen, in chemical shift of all elements, a jump change of the slope at the concentration of SiO_2 around 32 mole %. In this second part, the chemical shift stabilized on a constant value and the signal broadened progressively (FWHM ≈ 320 Hz). Additionally, NMR line shape changes from Lorentzian to Gaussian. It means that the local structure of the melt has, at the concentration of 32 mole % SiO_2, significantly changed. For the compounds that are tending to create glass phases, molecular motion (expressed by viscosity) is an important parameter. The width of the NMR peaks is one parameter that reflects that molecular motion. It is very sensitive to the rate of the molecular reorientation in liquid state [39]. The broadening of NMR lines, observed in our experiment, can currently be caused by the reduction of a solute's molecular mobility, which relates with the increase of the solution`s viscosity.

These findings are in very good agreement with the pivotal work made in this topic by Batashev and Zhurin in 1933 [29]. The authors have for the first time reported the phase diagram of the system Na_3AlF_6–SiO_2 (in the concentration range of SiO_2 from 0 to 50 wt. %). A eutectic point (coordinates; 3 wt.(10 mole) % SiO_2 and 980 °C) and an immiscibility field (above 12 wt. (32 mole) % SiO_2) was identified. This immiscibility phenomenon may exactly be responsible for the jump of the chemical shift observed in our experiment. Very similar findings can be also find in the work of Korenko *et al.* [19] where the investigation of the physico–chemical properties (density, viscosity and electrical conductivity) of the molten system Na_3AlF_6–SiO_2 can be found. The addition of silica to the molten cryolite had a big effect on the viscosity. The authors had assumed that a polymerized glassy–network formation in the melt is responsible for that behavior. Also, a sharp change in the excess molar volume and in the change of the trend of the electrical conductivity, detected at the concentration of SiO_2 very close to that reported by Batashev and Zhurin [29], were identified in the work of Korenko *et al.* [19].

An increase of the chemical shift of ^{27}Al can be also interpreted as a decrease of the average coordination number of the aluminum atoms. It means, that the increase of the SiO_2 content in the melt is related to the formation of four–coordinated aluminum $Al(O,F)_4$. A dissolution of alumina (Al_2O_3) and phosphate ($AlPO_4$) in cryolite melts was being previously studied by high temperature NMR and by MD simulations with DFT calculations [32, 34, 35]. The formation of fluoro–oxoaluminate and fluoro–aluminophosphate species, where aluminum atoms are connected by one or two Al−O−Al or P−O−Al bridges, was confirmed. Based on the similar chemical behavior of SiO_2 and $AlPO_4$, the dissolution of SiO_2 in molten Na_3AlF_6 could thus also be associated with the formation of oxygen containing bridges between aluminum and silicon Al−O−Si.

The fluorination of silica was more thoroughly assessed by Dolejš and Baker [40]. A complex quaternary system of Na_2O−Al_2O_3−SiO_2−F_2O_{-1} was investigated. In the binary Na_3AlF_6−SiO_2 space of this more complex system, a presence of the following chemical bonds and species were suggested: Al−O−Si (albite - $NaAlSi_3O_8$, nepheline - $NaAlSiO_4$, $Na_6Si_8O_{19}$), Al−Si−O−F (topaz - $Al_2SiO_4F_2$), and Na−Si−F (NaF, Na_2SiF_6, SiF_4(g)). The possible formation of Si–O–F bonds, similar to $SiO_2F_2^{2-}$ and $Si_2O_4F_3^{3-}$, was latter predicted by thermodynamic modeling in the molten systems containing Na, O, Si, and F atoms [41]. The presence of fluorine−containing alkali silicate glasses with Si−O−F tetrahedral is also reported in the following systems; MF−SiO_2 (M=alkali metals) and AlF_3−SiO_2 [42−43]. A $Si_4O_7F_2$−formation, was in these works, predicted as a reaction product.

In our measurements, the ^{19}F chemical shifts range from -191 to -198 ppm. This chemical shift, however, excludes the presence of Si−F, and Si−F−Na bounds groups in Na_3AlF_6–SiO_2 melts, since the ^{19}F chemical shift reported for Si−F−Na group (Na_2SiF_6) is at -152 ppm [44−45]. These authors, at the same time, proposed that the SiO_4−tetrahedron is preserved in the melt as a rigid structure entity. By the combination of the data, obtained for the different nuclei in our and previous works, we can propose that aluminium and silicon atoms in our melt would be connected by an Al−O−Si bridge.

A proper evidence for the previous statements can be seen when we look on Fig. 3. Let us simplify, that in pure molten Na_3AlF_6, the fluoroaluminate species−distribution (AlF_4^-, AlF_5^{2-}, and AlF_6^{3-}) is represent by AlF_5^{2-} as an average coordination form. Further, let us consider,

that the atomic fractions in the cryolite−rich melts (i.e. the partitioning of Al, F, and Si different species) can be derived by using the **Eqn. 1 and 2**. Then, one should notice, that for eutectic concentration, the ^{27}Al chemical shift moves upward (to the values corresponding to the pure albite (δ(^{27}Al) = 63.0ppm, for albite [46])), while the ^{19}F chemical shift remains the same. It means that at the eutectic composition, the fluorine partitioning between the different species in the solid and liquid phase, remains uniform.

3.2. Weight loss analysis

The experimental results of the mass losses are depicted in Fig 4. The mass loses were determined by weight analysis of the samples (after the melting and spontaneous cooling), as well as by X–ray fluorescence (XRF) analysis. The XRF analysis confirmed that the total

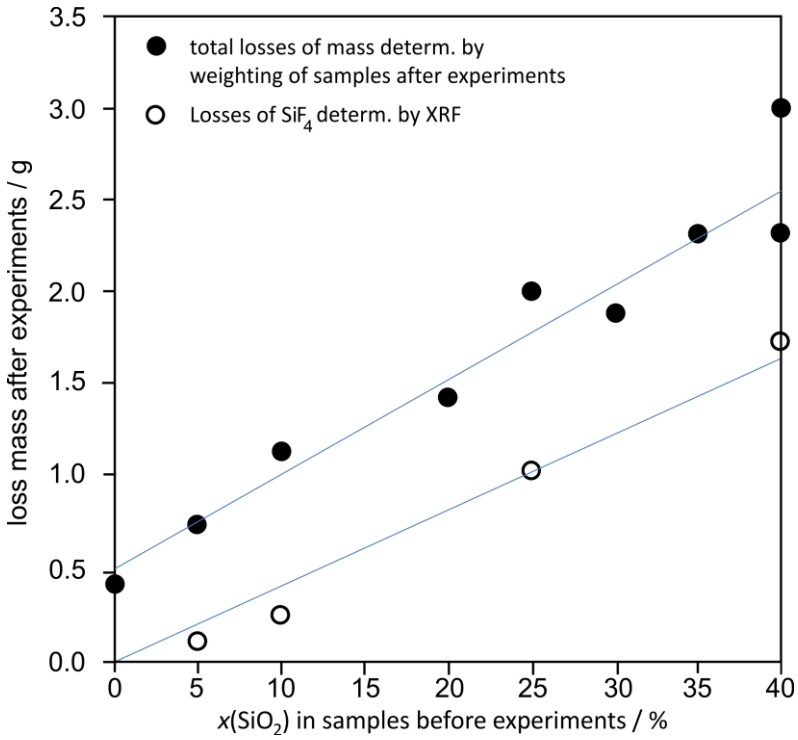

Fig. 4. A weight loss analysis in the system Na_3AlF_6–SiO_2. The amount of the samples: 30 g. Full circles: mass analysis after spontaneous cooling; open circles: SiF_4 losses determined by XRF analysis.

weight losses are in the linear relationship with the specific Si–losses, which is an indication that the weight losses are due to the volatilization of Si–compound(s) from the melt (e.g. SiF_4). The similar behavior was also found in the previous works [31, 40, 47−49] where the authors have reported SiF_4 as predominant volatile product, upon the melting of the mixture of Na_3AlF_6 and SiO_2. The formation of the volatile product shifts the melt`s composition from a simple binary system to the ternary system Na_3AlF_6−SiO_2−SiF_4. The continuous evaporation of SiF_4 off the melt further increases the thermodynamic degree of freedom and the system can then be considered, based on the Dolejš and Baker [40], as the quaternary Na_2O–Al_2O_3–SiO_2–F_2O_{-1} (using the Dolejš and Baker's formulas, suitable for the geological

description of granitic and rhyolitic magmas with the presence of fluorine). These authors also used a thermodynamic calculation to propose the following possible de–volatilization`s equilibria:

$$2Na_3AlF_6 + 4SiO_2 = SiF_4 + NaAlSi_3O_8 + 2NaF \quad (4)$$

or

$$2Na_3AlF_6 + 13SiO_2 = 3SiF_4 + 2NaAlSi_3O_8 + 2Na_2Si_2O_5 \quad (5)$$

To further zoom in the structural correlations in our molten system, especially at the melt/solid (glass) interphase, and to distinguish between the above–mentioned reaction paths, an application of a robust, cutting–edge approach was needed. A combined approach including the solid state NMR, XRD, and EDX analysis was applied. The solidified samples were prepared, either as spontaneously cooled, or as rapidly solidified (prepared by RSP).

3.3. Spontaneously solidified samples: X–ray and MAS NMR analysis

To be able to clarify an influence of the concentration of SiO_2 on the structure of the Na_3AlF_6–SiO_2 melt, a series of spontaneously solidified samples with different concentration of SiO_2 (5, 25 and 50 mole %) were prepared for a subsequent analysis.

An interesting phenomenon was visually observed when we looked at the solidified sample with the highest SiO_2 content (50 mole %). A formation of the two obviously separate and distinguish phases with different surface–look was visible. One phase looked like a "glass", while the other one had more "poly–crystalline" surface. Due to this fact, the sample with the content of SiO_2 50 mole % was analyzed by two ways:

i) as one single homogenized sample and

ii) as separated two phases, upper and lower layers.

The results from the first way of analysis are presented in this chapter 3.3. The results of the separated phases are reported in following chapter 3.4.

The Fig. 5 shows the results of the X–ray analysis of the spontaneously solidified samples. A MAS NMR (^{19}F, ^{23}Na, and ^{27}Al) analysis of those samples can be seen on the Fig. 6 and 7. A similar analysis of the separated phases (come from the sample with 50 mole % of SiO_2) is shown on the Fig. 8 and 9.

As it can be seen from the Fig. 5, two crystalline structures can be found in all spontaneously solidified samples of Na_3AlF_6–SiO_2. The first one is pure cryolite, the second one is NaF. A small part of NaF in the sample is from a well–known thermal dissociation of Na_3AlF_6 [50-52] according the following reaction.

$Na_3AlF_6(l) \rightarrow NaAlF_4(g) + 2NaF(l)$ (6)

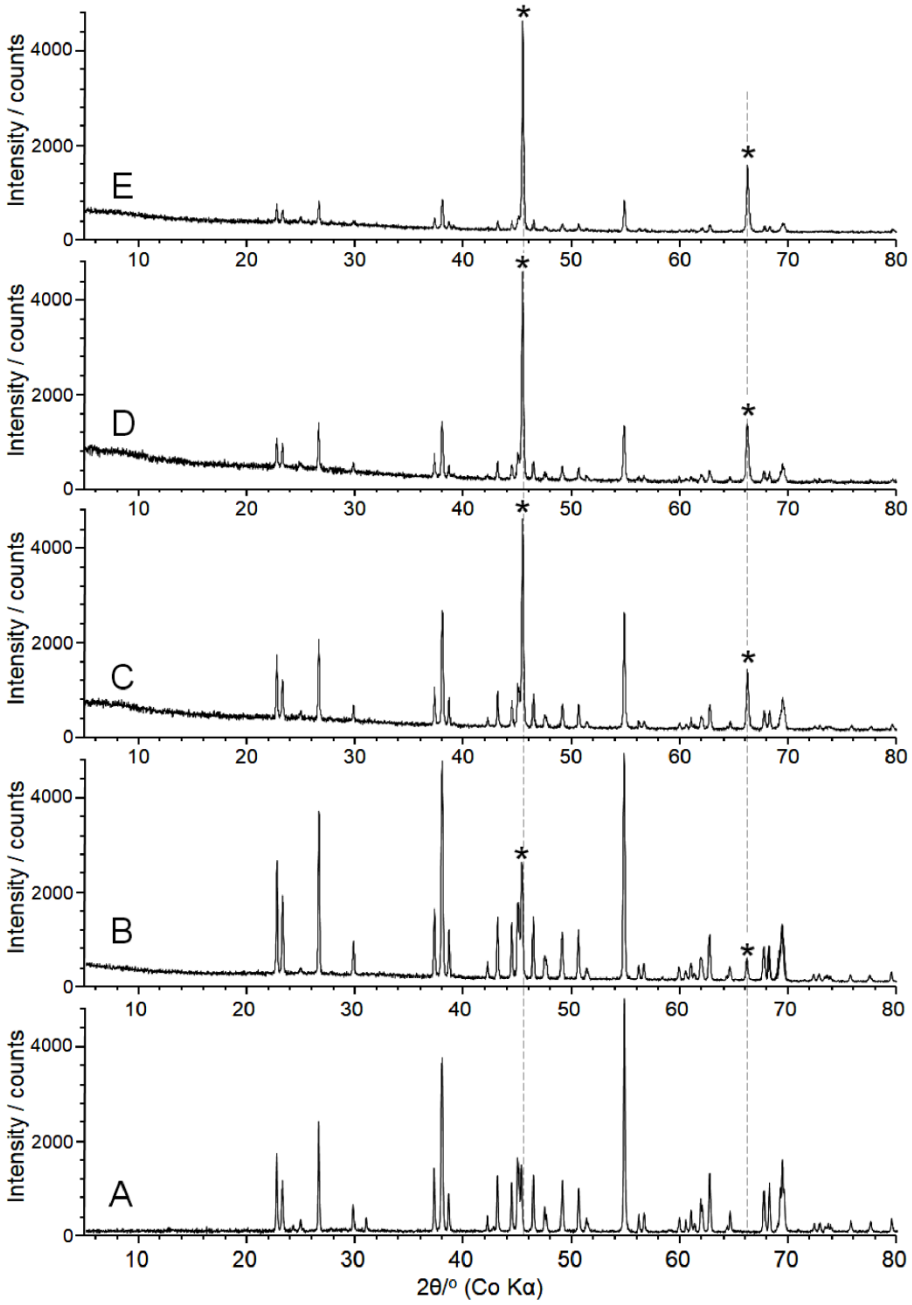

Fig. 5. The comparison of X-ray spectra of the spontaneously solidified samples with different content of SiO_2 (A – pure Na_3AlF_6 before melting [53, 54], B – pure Na_3AlF_6 after melting, C – 5 mole %, D – 25 mole % and E – 50 mole %); * – position of NaF diffractions [55, 56].

The rest of the NaF presented in the samples, comes from different possible reaction between cryolite and silica (e.g., like was proposed in work [4], and/or [40]). Other products

of the reactions can be in non–crystalline forms, or their patterns are covered by those of NaF. The non–crystalline forms were in fact detected in the sample with the higher concentration of silica (Fig. 5) where a typical background feature was observed in the range from 15° to 40° (2Θ). This background is typical for silicon glassy phases [57].

The intensity of NaF peaks however increase with the concentration of SiO_2, which means that the increasing presence of NaF in the samples can not only be a result of the thermal dissociation of cryolite. Some part of the newly formed NaF must be the product of the interaction between cryolite and silica. Another product(s) of the interaction between cryolite and silica ended up likely in outgoing vapors (like SiF_4), or in amorphous phase(s). Subsequent MAS NMR and SEM EDX analysis of the spontaneously and RSP rapidly solidified samples, was performed.

Figure 6 shows the high resolution ^{19}F, ^{23}Na, and ^{27}Al MAS NMR spectra of the spontaneously solidified samples. As it can be seen from the figure, the fluorine spectra

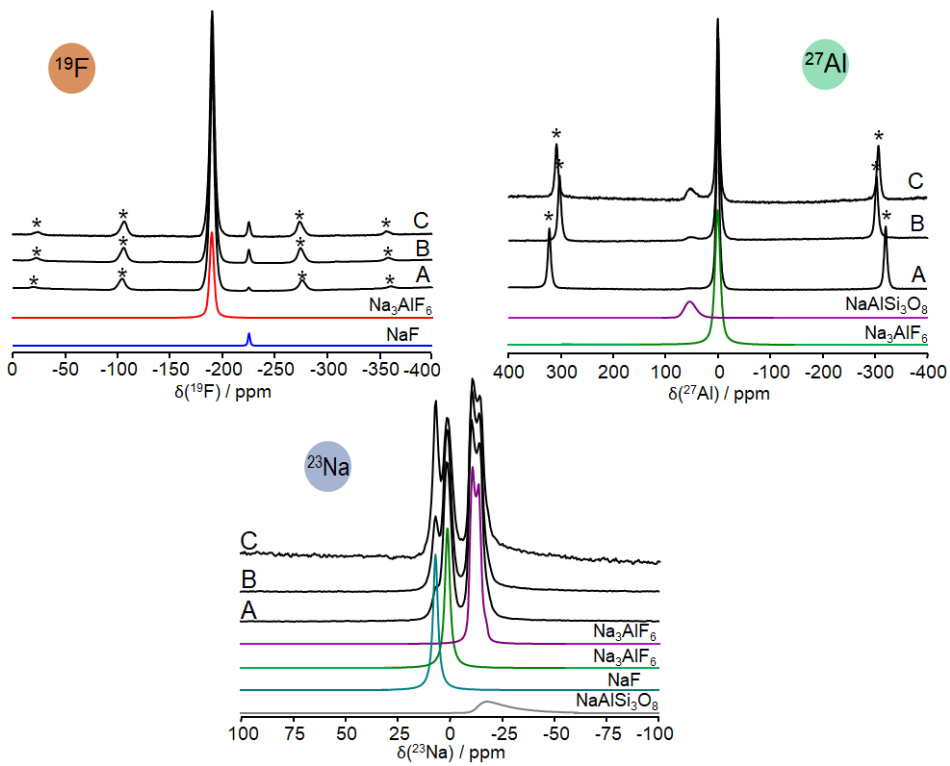

Fig. 6. The comparison of ^{19}F, ^{23}Na, and ^{27}Al spectra (black lines) of the spontaneously solidified samples with different content of SiO_2 (A – 5 mole %, B – 25 mole % and C – 50 mole %); * – spinning side bands. Colored lines show the contributions of each fitting component.

of all samples contained only two signals; one at -191 ppm and another at -223 ppm. The first signal is assigned to cryolite (Na_3AlF_6), while the second signal to sodium fluoride (NaF). The intensity of the peak belongs to the NaF increases with the increasing concentration of SiO_2 in the samples. This observation is another evidence that the major amount of NaF in

this system comes from the reaction between molten Na_3AlF_6 and SiO_2. The absence of other fluorine signals in samples also indicates that no other compounds, with the fluorine atom in their structure, are present in the melt. This finding is in agreement with the HT NMR results.

In the case of ^{27}Al NMR, the spectra of all samples contain a signal at 0 ppm corresponds to the aluminum in the octahedral structure of cryolite (Na_3AlF_6). The spectra also contain a new signal at (δ_{iso} = - 56 ppm). The intensity of that signal is clearly increasing with the concentration of SiO_2 in the samples. But the shape of this peak indicates, that this compound is amorphous; hence, likely does not belong to any crystalline phase [58]. The ^{23}Na spectra contain peaks at 7 ppm and at 1.7 ppm, and one duplet at 7.8 ppm. The first peak ascribed to sodium in NaF, we can again see the increasing of its intensity with the increasing of the concentration of SiO_2 in the samples. Two other peaks correspond to the sodium, intercalated into two positions in the structure of cryolite (Na_3AlF_6). An increase of the background of these spectra can be also seen, especially at the highest concentration of the SiO_2, indicating a presence of a disordered compound, amorphous $NaAlSi_3O_8$ [59]. This fact was the very reason why a convolution of the ^{23}Na spectra was subsequently performed (Fig. 7).

Based on what was already said above, we can conclude that the increasing of the concentration of SiO_2 brings about two major effects in the spontaneously solidified samples of the system Na_3AlF_6–SiO_2. The first effect is related to the reaction between both components where one of the product is NaF (e.g. based on the reactions 1, 2 or 4). The second effect, especially pronounced at higher concentration of SiO_2, is a presence of disordered amorphous compound/compounds. Both findings are in very good correlation with what was already observed in the X–ray analysis of this system.

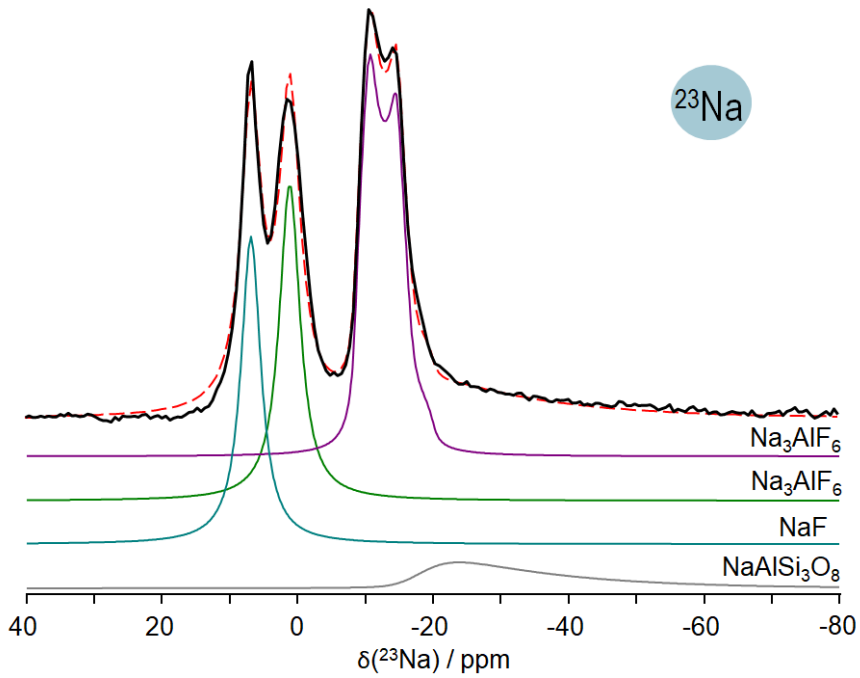

Fig 7. ^{23}Na MAS NMR spectrum of spontaneously solidified sample with 50 mole %. SiO_2: black line experimental, red dotted line are fitted spectra, colored lines show the contributions of each fitting component.

3.4. X–ray and MAS NMR analysis of the sample with 50 mole % SiO_2

Figure 8 shows an X–ray diffraction of separable phases of the sample SiO_2 that was prepared with 50 mole %, as was mentioned above. The upper crystalline layer (Fig. 8 upper pattern) contains only NaF and cryolite. The lower polycrystalline layer (Fig. 8, lower pattern) contains only the diffractions of cryolite and the diffractions of tridymite and cristobalite. Tridymite is β– form of SiO_2,

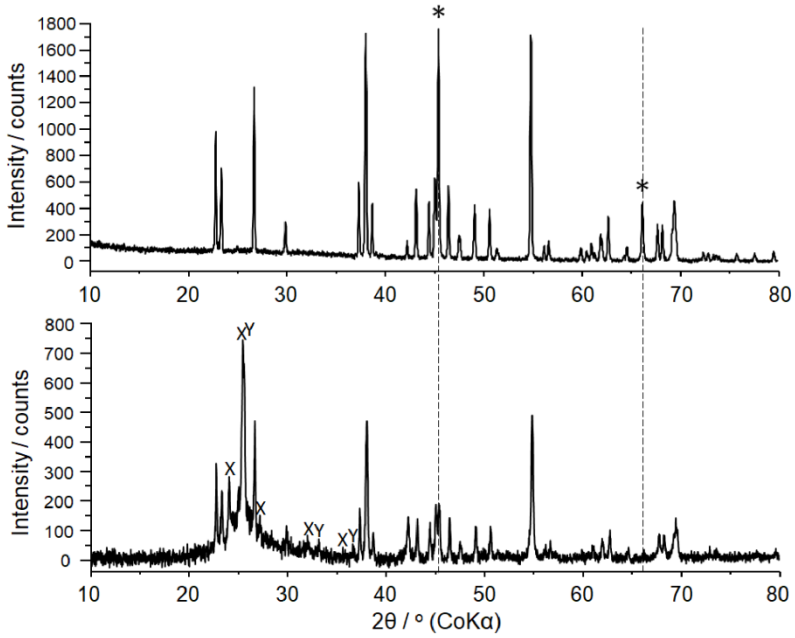

Fig. 8. X-ray pattern of the Na_3AlF_6 mixture with 50 mole % of SiO_2; picture up - upper crystalline layer of the sample (*– NaF [55, 56], other diffractions – Na_3AlF_6 [53, 54]); picture down - lower polycrystalline layer of the sample (X – SiO_2 (cristobalite form) [60], Y – SiO_2 (tridymite form) [61]).

while cristobalite is γ– form of this compound. These findings are in line with the work of [40], where is reported the existence of a large stability fields of the silica polymorphs in the silica–fluoride systems. These structures of silica had been mostly identified on the typical non–crystalline background feature, observed in the range from 15° to 40° (2Θ). The feature in this range represents a wide interval of Gaussian distribution of bound distance between silicon and oxygen in the structure of SiO_2. According to the diffraction pattern in this region (20° − 40°, 2Θ), the new glassy phases in this system are probably based on cristobalite and tridymite (β– and γ– form of SiO_2). The spectrum of the lower layer also contains some minor diffractions of Na_3AlF_6 and NaF.

The presence of the liquid–liquid immiscibility in molten fluoride–silicates has been a matter of a long discussion [24, 28−29, 62]. The last investigations are indicating [40] that the immiscibility phenomenon exists in these systems only at higher temperatures (1200 °C) and/or higher pressures (600 MPa). No immiscibility below 1100 °C was confirmed [40]. To

elucidate the structure of the amorphous phase/phases, identified by X−ray diffraction, a MAS NMR spectroscopy (^{27}Al, ^{19}F, ^{23}Na, and ^{29}Si) of the lower layer was performed, as well (Figure 9).

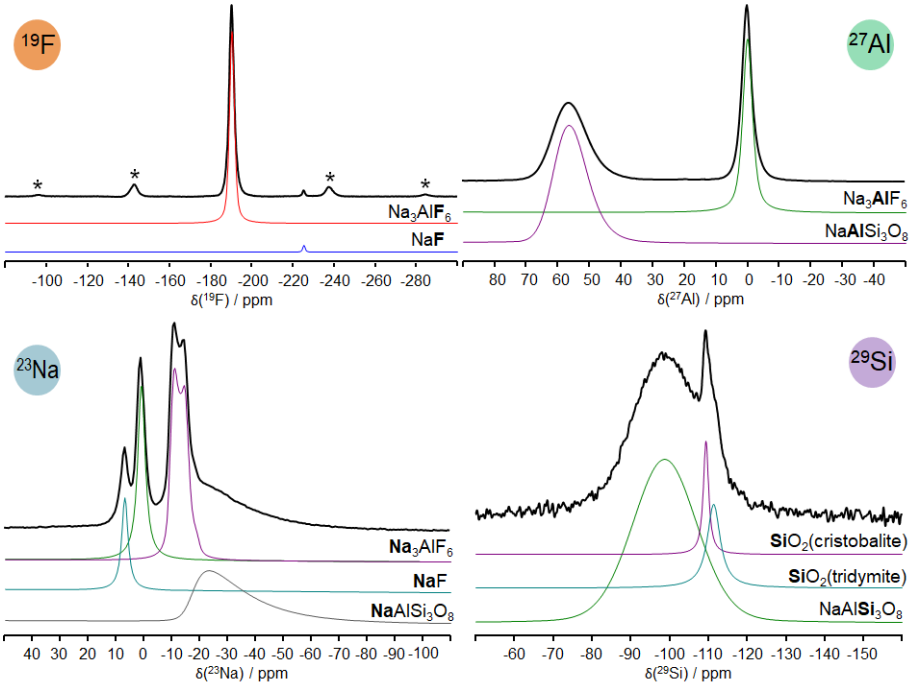

Fig 9. The fit of the MAS NMR (^{19}F, ^{27}Al, ^{23}Na and ^{29}Si) of the lower layer of the spontaneously solidified Na_3AlF_6 mixture with 50 mole % of SiO_2.

As it can be seen in Fig. 9, the spectra of the ^{19}F and ^{23}Na isotopes contain peaks assigned to the crystal structure of Na_3AlF_6 and NaF. The spectrum of the ^{27}Al isotope contains, beside a peak with δ_{iso} = 0 ppm assigned to six−coordinated octahedral species (AlF_6) in the structure of Na_3AlF_6, also a broad peak at δ_{iso} = 56 ppm assigned to tetrahedral framework of AlO_4. If we compare the peak positions of the ^{27}Al, ^{23}Na, and ^{29}Si with the positions of those nuclei in one type of glass forming alumino–silicate, albite ($NaAlSi_3O_8$), a very good correlation of the positions of those nuclei can be obtained. The presence of amorphous phase confirms also a relative width of the peaks of $NaAlSi_3O_8$ which is due to a range of bond angles and bond distances around Al−O−Si sites [63, 64]. The tetrahedral framework of AlO_4, identified in the ^{27}Al spectrum (peak at δ_{iso} = 0 ppm) is very likely related with albite as well. The ^{29}Si NMR spectra contains a broad peak assigned to $NaAlSi_3O_8$ and a relatively sharp peak of SiO_2 in the mixed form of cristobalite and tridymite. The presence of these forms of SiO_2 in the samples was already confirmed by X–ray analysis. The ^{19}F spectrum contains, besides the peaks already assigned to Na_3AlF_6, only a small resonance of NaF. This fact indicates that the amorphous phase in the upper layer of the sample does not contain any species with fluorine.

Based what was found, it can be concluded that in molten system of Na_3AlF_6–SiO_2, a reaction occurs between constituents. The products of the reaction between Na_3AlF_6 and SiO_2 are NaF, $NaAlSi_3O_8$, and very likely (assuming atmospheric pressure) also vapors of SiF_4.

These conclusions are in a good agreement with one of the thermodynamic models (Eqn. 4) proposed by Dolejš and Baker [40].

3.5. Rapidly solidified samples - SEM and EDX analysis

In order further probe the structural correlations and the chemistry of the studied system of Na_3AlF_6–SiO_2, a rapid solidification processing (RSP) was used to prepare deeply under–cooled samples with 25 and 50 mole % of SiO_2. Figure 10 shows a morphology of the surface, as well SEM EDX analysis on some identified spots on the surface of the under–cooled samples. As can be seen, the morphology of the samples is quite different from one another.

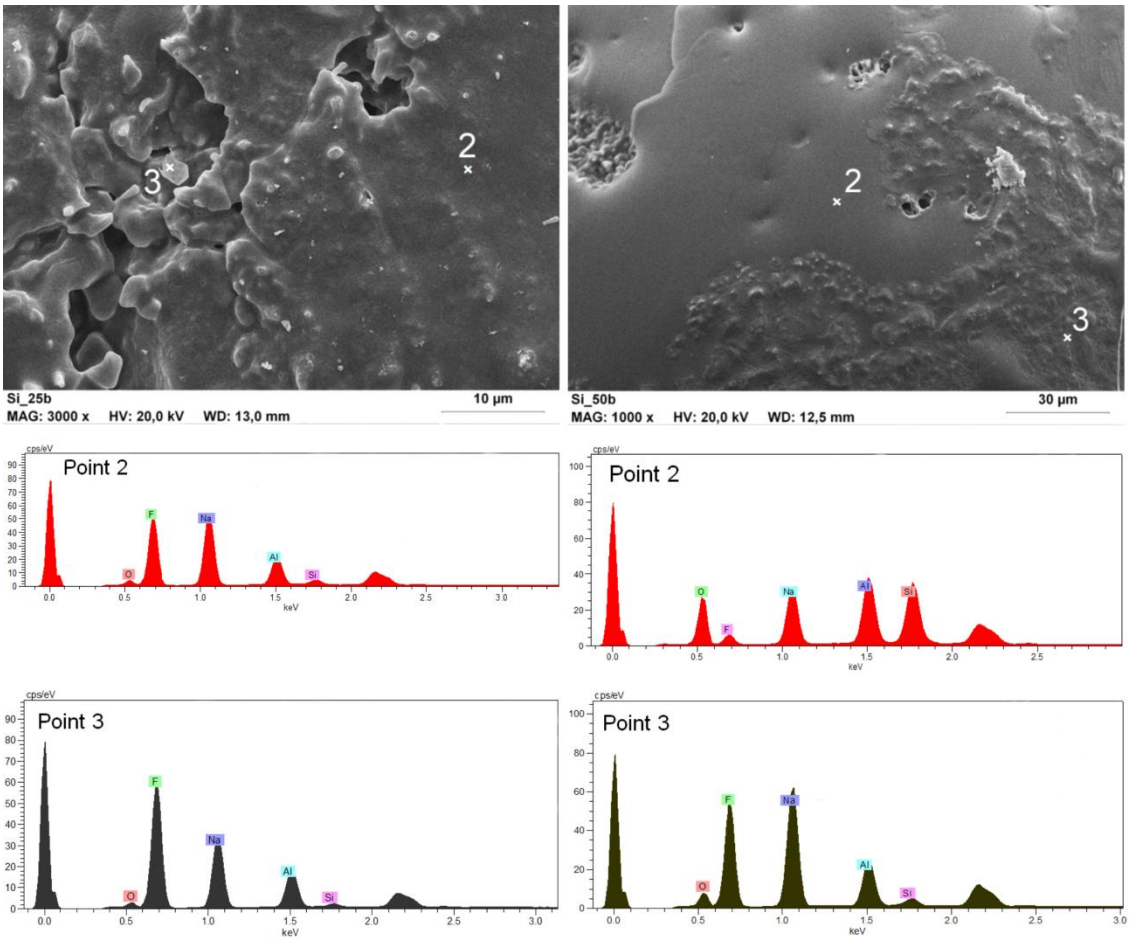

Fig. 10. SEM EDX analysis of the deeply under–cooled samples of Na_3AlF_6–SiO_2 system (25 and 50 mole % SiO_2) prepared by RSP. The left side: 25 mole % of SiO_2. The right side: 50 mole % of SiO_2.

The sample on the left side (25 mole % of SiO_2) consists of a uniform "spongy" morphology with hindered crystal growth. The morphology of the sample on the right side (50 mole % of SiO_2) is different, and two separable phases are clearly visible. All related elements (Na, Al, O, Si, and F), although in different concentration, was found to be present in all analyzed spots in both samples. However, the figure shows that the smooth phase in the sample on the right side (50 mole % of SiO_2) has somewhat higher concentration of oxygen, aluminum and

silicon. The increased concentration of these elements may relate with the presence of $NaAlSi_3O_8$ in this phase. On the other hand, the SEM EDX analysis of more rough phase (spots 2 and 3 on the left side and spot 3 on right side) shows a higher concentration of sodium and aluminum, which is probably related with the higher content of NaF and Na_3AlF_6.

The analysis of rapidly solidified sample with higher concentration of silica (50 mole %) proved what had been already indicated by previous analysis that the higher concentration of SiO_2 in Na_3AlF_6 – SiO_2 system lead to polymerization of the melt and the formation of albite $NaAlSi_3O_8$.

4. Conclusion

NMR analysis of Na_3AlF_6–SiO_2 melts and solidified melts by means of the selective observation of the different nuclei involved in the system (^{19}F, ^{27}Al, ^{23}Na and ^{29}Si), and coupled with the side X–ray diffraction, showed to be a powerful tool for the phase/structural description of such a complex systems. We would like to stress that it was, to our knowledge, for the first time when NMR technique was used for the high temperature analysis of this rather complicated molten/crystallized (amorphous) Na_3AlF_6–SiO_2 system. It can be finally concluded, that in molten system of Na_3AlF_6–SiO_2, a formation of NaF, $NaAlSi_3O_8$, and SiF_4 occurs. The silicon anion is incorporated into the melt structure by the Al–O–Si oxygen bridge. The high temperature reaction, which leads to this formation, can be formally described with the following scheme.

$$Na_3AlF_6(l) + 4\ SiO_2(diss) = 2\ NaF(l) + NaAlSi_3O_8(l) + SiF_4(g) \qquad (7)$$

The X–ray, SEM EDX analysis and MAS NMR analysis of the spontaneously and rapidly solidified samples also showed that the composition of the products on the right side of the reaction (7) does not change upon precipitation. The solidified samples retained the similar constituents like in the molten state: NaF, albite, cristobalite, trydimite and an amorphous phase(s) derived from the different modifications of SiO_2.

Ackowledgement

This study was financially supported by the Slovak bilateral project (N° SK–FR–2013–0039), and Slovak Grant Agencies (VEGA–2/0060/18). The work performed within the ITMS project (with code 313021T081) supported by Research & Innovation Operational Programme funded by the ERDF.

References

[1] Technology Roadmap: Solar Photovoltaic energy, Energy Technology Perspectives. http://mdvseia.org/wp-content/uploads/2015/05/Technology-Roadmap-Solar-PV-2014-version.pdf, 2014.

[2] Z. Chen, W. Ma, J. Wu, K. Wei, X. Yang, G. Lv, K. Xie, J. Yu, Influence of carbothermic reduction on submerged arc furnace energy efficiency during silicon production. Energy 116 (2016) 687−693.

[3] Z. Chen, W. Ma, K. Wei, S. Li, W. Ding, Effect of raw materials on the production process of the silicon furnace. J. Clean. Prod. 158 (2017) 359−366.

[4] G. Boe, K. Grjotheim, K. Matiašovský, P. Fellner, "Electrolytic Deposition of Silicon and of Silicon Alloys Part II: Decomposition Voltages of Components and Current Efficiency in the Electrolysis of the Na_3AlF_6-Al_2O_3-SiO_2 Mixtures, Can. Met. Quart. 10 (1971) 179–183.

[5] K. Matiašovský, M. Malinovský, V. Daněk, Specific electrical conductivity of molten flourides, Electrochim. Acta 15 (1970) 25–32.

[6] U. Cohen, Some prospective applications of silicon electrodeposition from molten fluorides to solar cell fabrication, J. Electron. Mater. 6 (1977) 607–643.

[7] T. Oishi, M. Watanabe, K. Koyama, M. Tanaka, K. Saegusa, Process for Solar Grade Silicon Production by Molten Salt Electrolysis Using Aluminium–Silicon Liquid Alloy, J. Electrochem. Soc.158 (2011) E93–E99.

[8] L. Famiyeh, Electrodeposition of Silicon in Fluoride Melts, *PhD. Thesis*, Norwegian University of Sciences and Technology (NTNU), 2011.

[9] S. Sokhanvaran, S. Thomas, M. Barati, Charge transport properties of cryolite–silica melts, Electrochim. Acta 66 (2012) 239−244.

[10] S.K. Cho, F.F. Fan, A.J. Bard, Formation of a silicon layer by electroreduction of SiO_2 nanoparticles in $CaCl_2$ molten salt, Electrochim. Acta 65 (2012) 57−63.

[11] A.L. Bieber, L. Massot, M. Gibilaro, L. Cassayre, P. Taxil, P. Chamelot, Silicon electrodeposition in molten fluorides, Electrochim. Acta 62 (2012) 282−289.

[12] E. Ergul, I. Karakaya, M. Erdogan, Electrochemical decomposition of SiO_2 pellets to form silicon in molten salts, J. Alloys Compd. 509 (2011) 899−903.

[13] A.H. Abbar, S.H. Kareem, F.A. ALSaady, Electrodeposition of Silicon from Fluorosilicic Acid Produced in Iraqi Phosphate Fertilizer Plant, J. Electrochem. Sci. Technol. 2 (2011) 168−173.

[14] X. Zou, H. Xie, Y. Zhai, X. Lang, Direct Synthesis of High Purity Silicon Wires by Electrorefining in Molten KF–NaF Eutectic, Chin. J. Chem. Phys. 26 (2013) 88–94.

[15] J. Xu, G.M. Haarberg, Electrodeposition of Solar Cell Grade Silicon in High Temperature Molten Salts, High Temp. Mater. *Proc.* 32 (2013) 97–105.

[16] S.M. Thomas, Study of Properties of Cryolite – Lithium Fluoride Melt containing Silica, PhD Thesis, Materials Science and Engineering, University of Toronto, 2012.

[17] L. Massot, A.L.Bieber, M. Gibilaro, L. Cassayre, P. Taxil, P. Chamelot, Silicon recovery from silicon-iron alloys by electrorefining in molten fluorides, Electrochim. Acta 96 (2013) 97–102.

[18] L. Li, J. Guan, A. Liu, Zh. Shi, M. Korenko, J. Xu, B. Gao, Zh. Wang, Preparation of Solar Grade Silicon Precursors by Silicon Dioxide Electrolysis in Molten Salts, The Minerals, Metals and Materials Society - TMS, EPD Congres, 2015.

[19] M. Korenko, Z. Vasková, J. Priščák, F. Šimko, M. Ambrová, Zh. Shi, Density, Viscosity and Electrical Conductivity of Molten Cryolite Electrolytes (Na_3AlF_6–SiO_2) for Solar Grade Silicon (Si-SoG) Electrowinning, Silicon 7 (2015) 261–267.

[20] J. Young, Solid Oxide Membrane (SOM) Process for Ytterbium and Silicon Production from their Oxides, *PhD Thesis*, Boston University (BU), 2015.

[21] E. Juzeliūnas, D.J. Fray, Silicon Electrochemistry in Molten Salt, Chem. Rev. 120 (2020) 1690−1709.

[22] R. Monnier, J.G. Giacometti, Recherches sur le raffinage électrolytique du silicium, Helv. Chim. Acta 47 (1964) 345−353.

[23] R. Monnier, D. Barakat, Dual Cell Refining of Silicon and Germanium. Gen Trustee Company Inc., US patent 3,219,561 (23 Nov. 1965) and US patent 3,254,010 (31 May 1966).

[24] K. Grjotheim, K. Matiašovsky, P. Fellner, A. Silný, Electrolytic deposition of silicon and silicon alloys: Part I: Physicochemical properties of the Na_3AlF_6–Al_2O_3–SiO_2 mixtures, Can. Metall. Q. 10 (1971) 79−82.

[25] K. Grjotheim, K. Matiašovsky, P. Fellner, The electrodeposition of silicon from cryolite melts. Light Met. 1982 (1982) 333−341.

[26] A.I. Belyaev, Physicochemical processes at electrolysis of aluminium; Metallurgizdat, Moscow, Russia, 1947. (*in Russian*)

[27] S. Sokhanvaran, S. Thomas, M. Barati, Charge transport properties of cryolite−silica melts, Electrochim. Acta 66 (2012) 239–244.

[28] D.F. Weill, W.J. Fyfe, The 1010 ° and 800 °C isothermal section in the system, J. Electrochem. Soc. 111 (1964) 582−589.

[29] K.P. Batashev, A.I. Zhurin, Metallurg. 66(2) (1933) 66−72; (Citation according to: G.A. Abramov, M.M. Vetjukov, I.P. Gupalo, A.A. Kostjukov, L.I. Lozkin, Teoreticeskoye Osnovy Elektrometallurgii Alyuminiya. Metallurgizdat, Moscow, 1953, p. 502).

[30] K. Grjotheim, K. Matiašovský, P. Fellner, Electrolytic Preparation of the Al−Si Alloy. Proceeding of the IV Al Symphosium, 16-18.11.1980, Banská Bystrica, Slovakia.

[31] P. Fellner, K. Matiašovský, Chemical reactions in molten Na_3AlF_6−SiO_2−Al_2O_3−AlF_3 mixtures. Chem. Pap. 27 (1973) 737−741.

[32] K. Machado, D. Zanghi, M. Salanne, V. Stabrowski, C. Bessada, Anionic Structure in Molten Cryolite–Alumina Systems, J. Phys. Chem. C 122 (2018) 21807−21816.

[33] A. Rakhmatullin, K. Machado, D. Zanghi, I.B. Polovov, R. Bakirov, K.V. Maksimtsev, C. Bessada, Study of the $NaF-ScF_3$ system as a molten bath for production of Sc alloys: A combination of NMR and molecular dynamics simulations. J. Alloys Compd. 786 (2019) 953−959.

[34] M. Keppert, A. Rakhmatullin, F. Šimko, M. Deschamps, G.M Haarberg, C. Bessada, Multi- nuclear magnetic resonance study of $Na_3AlF_6-AlPO_4$ molten and solidified mixtures, Magn. Reson. Chem. 46 (2008) 803–810.

[35] A. Rakhmatullin, M. Keppert, F. Šimko, C. Bessada Aluminium phosphate behaviour in Na_3AlF_6-Al_2O_3 melts: a new insight from in situ high temperature NMR measurements New J. Chem. 40 1737−1741

[36] A.L. Jacobson, J. McKittrick, Rapid solidification processing, Mater. Sci. Eng. R11 (1994) 355–408.

[37] E.J. Lavernia, T.S. Srivatsan, The rapid solidification processing of materials: science, principles, technology, advances, and applications, J. Mater. Sci. 45 (2010) 287–325.

[38] D. Massiot, F. Fayon, M. Capron, I. King, S. Le Calve, B. Alonso, J. O. Durand, B. Bujoli, Z. Gan, G. Hoatson, Modelling one and two-dimensional solid-state NMR spectra. Magn. Reson. Chem. 40 (2002) 70−76.

[39] S.J. Anderson *Nuclear Magnetic Resonance Spectroscopy in Environmental Chemistry*. Oxford Univ. Press, Inc., New York, US, 1997, p. 58.

[40] D. Dolejš, D.R. Baker, Thermodynamic analysis of the system $Na_2O-K_2O-CaO-Al_2O_3-SiO_2-H_2O-F_2O_{-1}$: Stability of fluorine-bearing minerals in felsic igneous suites, Contrib. Mineral. Petr. 146 (2004) 762−778.

[41] D. Dolejš, D.R. Baker, Thermodynamic modeling of melts in the system $Na_2O-NaAlO_2-SiO_2-F_2O_{-1}$, Geochim. Cosmochim. Acta 69 (2005) 5537−5581.

[42] N. Takusagawa, Infrared Absorption Spectra and Strucutre of Fluorine-Containing Alkali Silicate Glasses, J. Non-Cryst. Solids 42 (1980) 35−40.

[43] B.O. Mysen, D. Virgo, Interaction Between Fluorine and Silica in Quenched Melts on the Joins SiO_2-AlF_3 and SiO_2-NaF Determined by Raman Spectroscopy, Phys. Chem. Miner. 12 (1985) 77−85.

[44] Q. Zeng, J.F. Stebbins, Fluoride sites in aluminosilicate glasses: High-resolution ^{19}F NMR results, Am. Mineral 85 (2000) 863–867.

[45] T.M. Duncan, D.C. Douglass, R. Csencsits, K.L. Walker, Study of Fluorine in Silicate Glass with ^{19}F Nuclear Magnetic Resonance Spectroscopy, J. Appl. Phys. 60 (1986) 130–136.

[46] J.F. Stebbins, Nuclear Magnetic Resonance Spectroscopy of Silicates and Oxides in Geochemistry and Geophysics. Mineral Physics & Crystallography: A Handbook of Physical Constants, 1995, 303–331.

[47] L.N. Kogarko, L.D. Krigman, N.S. Sharudilo, Experimental investigation of the effect of alkalinity of silicate melts on the separation of fluorine into the gas phase, Geochem. Int. 5 (1968) 782–790.

[48] R.J. Snow, B.J. Welch, Reactions in the cryolite–silica system, Proceedings of the Australasian Institute of Mining and Metallurgy 241 (1972) 81−85.

[49] O-J. Siljan, Sodium aluminium fluoride attack on alumino-silicate refractories—chemical reactions and mineral formation, Dr-Ing. thesis, Trondheim, Norwegian University of Science and Technology, 1990, p. 274.

[50] K. Grjotheim, C. Krohn, M. Malinovský, K. Matiašovský, and J. Thonstad, Aluminium Electrolysis - Fundamentals of Hall-Héroult Process, 2nd ed., Alminium Verlag, Dusseldorf, 1982.

[51] K. Grjotheim, B. Welsh, Aluminium Smelter Technology: A Pure and Applied Approach, Aluminium Verlag, Dusseldorf, 1988.

[52] J. Thonstad, P. Fellner, G.M. Haarberg, J. Híveš, A. Kvande, and A. Sterten, Aluminium Electrolysis - Fundamentals of Hall-Héroult Process, 3rd ed., Alminium Verlag, Dusseldorf, 2001.

[50] F.C. Hawthorne, R.B. Ferguson, Refinement of the Crystal Structure of Cryolite, Can. Mineral. 13 (1975) 377−382.

[51] H. Yang, S. Ghose, D.M. Hatch, Ferroelastic Phase Transition in Cryolite, Na_3AIF_6, a Mixed Fluoride Perovskite: High Temperature Single Crystal X-ray Diffraction Study and Symmetry Analysis of the Transition Mechanism, Phys. Chem. Minerals 19 (1993) 528−544.

[52] V.T. Deshpande, Thermal expansion of sodium fluoride and sodium bromide, Acta Crystallogr. 14(7) (1961) 794–794.

[53] H.F. McMurdie, M.C. Morris, E.H. Evans, B. Paretzkin, W. Wong-Ng, L. Ettlinger, C.R. Hubbard, Standard X-Ray Diffraction Powder Patterns from the JCPDS Research Associateship, Powder Diffr. 1 (1986) 64–77.

[54] M.C. Mascolo, G. Dell'Agli, C. Ferone, M. Pansini, G. Mascolo, Thermal crystallization of ion-exchanged zeolite A, J. Eur. Ceram. Soc. 23 (2003) 1705–1713.

[55] J.-B. D' Espinose de Lacaillerie, C. Fretigny, D. Massiot, MAS NMR spectra of quadrupolar nuclei in disordered solids: The Czjzek model, J. Magn. Res. 192(2) (2008) 244–251.

[56] C. E. Schmelz, J. F. Stebbins, Gel synthesis of an albite ($NaAlSi_3O_8$) glass: An NMR analysis, Geochim. Cosmochim. Acta 57(16) (1993) 3949–3960.

[57] D. Hanawalt, H.W. Rinn, L.K. Frevel, Chemical Analysis by X-Ray Diffraction, Anal. Chem. 10 (1938) 475−512.

[58] E. Smelik, R. Reeber, R. A study of the thermal behavior of terrestrial tridymite by continuous X-ray diffraction, Phys. Chem. Miner 17 (1990) 197−206.

[59] L.N. Kogarko, L.D. Krigman, Unmixing in fluorosilicate systems, Phys. Chem. Glasses 1 (1975) 61−65 (*in Russian*).

[60] J.B. Murdoch, J.F. Stebbins, I.S.E. Carmichael, High-resolution ^{29}Si NMR study of silicate and aluminosilicate glasses: the effect of network-modifying cations, Am. Mineral 70 (1985) 332–343.

[61] R.J. Kirkpatrick, R.A. Kinsey, K.A. Smith, D.M. Henderson, E. Oldfield, High resolution solid-state sodium-23, aluminum-27, and silicon-29 nuclear magnetic resonance spectroscopic reconnaissance of alkali and plagioclase feldspars, Am. Mineral 70 (1985) 106–123.